THE JOURNAL OF PHYSICAL CHEMISTRY B

ARTICLE

pubs.acs.org/JPCB

Direct Observation of Vibrational Energy Flow in Cytochrome *c*

Naoki Fujii, Misao Mizuno, and Yasuhisa Mizutani*

Department of Chemistry, Graduate School of Science, Osaka University, 1-1 Machikaneyama, Toyonaka, Osaka 560-0043, Japan

Supporting Information

ABSTRACT: Vibrational energy flow in ferric cytochrome *c* has been examined by picosecond time-resolved anti-Stokes ultraviolet resonance Raman (UVRR) measurements. By taking advantage of the extremely short nonradiative excited state lifetime of heme in the protein (≪ ps), excess vibrational energy of 20000−25000 cm^{-1} was optically deposited selectively at the heme site. Subsequent energy relaxation in the protein moiety was investigated by monitoring the anti-Stokes UVRR intensities of the Trp59 residue, which is a single tryptophan residue involved in the protein that is located close to the heme group. It was found from temporal changes of the anti-Stokes UVRR intensities that the energy flow from the heme to Trp59 and the energy release from Trp59 took place with the time constants of 1−3 and ∼8 ps, respectively. These data are consistent with the time constants for the vibrational relaxation of the heme and heating of water reported for hemeproteins. The kinetics of the energy flow were not affected by the amount of excess energy deposited at the heme group. These results demonstrate that the present technique is a powerful tool for studying the vibrational energy flow in proteins.

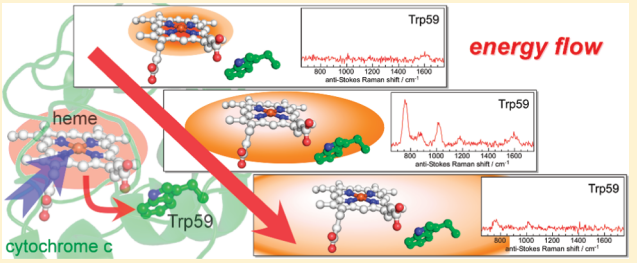

INTRODUCTION

The problem of vibrational energy relaxation is of central importance for understanding chemical dynamics in solution because the rates and pathways of condensed phase chemical reactions are intimately connected with the ability of the reactants to exchange energy with the surrounding solvent. Vibrational energy relaxation has been investigated from many different standpoints.[1−6] Considerable attention has been attracted to the relaxation in protein. Energy exchange in the many degrees of freedom in proteins is an important process in their functioning.[7−13] The dynamics of energy exchange between these different degrees of freedom determines the fluctuation and dissipation processes that govern the protein's motion and is central to understanding how energy is transduced from a stimulus into motion. The energy redistribution can be followed by monitoring both the decay of the initially excited mode(s) and the buildup of energy in the accepting modes. With this approach, it is possible to spatially and temporally map the energy flow pathways in proteins.

Hemeproteins are ideal systems to study the vibrational energy flow in proteins. The heme group is relatively isolated from the rest of the protein and approximates a solute in solution. By taking advantage of the extremely short nonradiative excited state lifetime of heme in proteins (≪ ps),[14] it is possible to optically deposit about 20000 cm^{-1} of excess vibrational energy selectively at the heme site fast enough to resolve the subsequent energy redistribution processes. For this initial condition, the vibrational modes of the heme group, the surrounding protein matrix, and highly damped collisional modes of the water can be used as a basis set to discuss the energy flow in the protein.[10,11,15]

Time-resolved resonance Raman studies[16−19] and power dependencies of the Stokes and anti-Stokes modes of the heme group[20] have determined that the transfer of energy from the vibrationally excited heme to the surrounding protein moiety occurs with time constants on the order of a few picoseconds. The released energy from the heme diffuses inside the protein and finally goes out to the water. The fast energy dissipation from the protein moiety to the water bath has also been noted by femtosecond time-resolved IR studies, which involved monitoring the heating of water that resulted from photoexcitation of myoglobin.[21] The observed kinetics were fitted with a model having two time constants. The fast component was best fitted by a Gaussian rise function with a time constant of 7.5 ± 1.5 ps, and the slow component was described by a time constant of ∼20 ps with 40% of the total amplitude. Transient grating studies determined that most of the energy is dissipated from the protein into the aqueous bath in less than 22 ps.[22,23] Thus, the time scales of energy relaxation of the heme group and energy dissipation from the protein moiety to water have been well characterized. However, no direct observation has been done, and little is known about energy flow in proteins.

To address this issue, we used time-resolved anti-Stokes ultraviolet resonance Raman (UVRR) spectroscopy to monitor the vibrationally excited population in an amino acid residue following photoexcitation of the heme group. Time-resolved anti-Stokes Raman spectroscopy is selective for vibrationally excited

Received: August 5, 2011
Revised: September 28, 2011
Published: October 05, 2011

populations and therefore is powerful for measuring vibrational energy transfer.[5,18] This technique has the advantage that many vibrational transitions in a wide frequency range can simultaneously be observed with a single probe frequency. In addition, the resonance effect allows us to measure the vibrational spectra of the solute without severe solvent interference. Furthermore, UVRR spectroscopy is a useful technique for studying the structure and dynamics of proteins because the vibrational bands of the aromatic amino acid side chains in proteins are selectively enhanced,[24,25] and the pump−probe method using pulses in the picosecond range enables us to study ultrafast protein dynamics. We have recently constructed a picosecond time-resolved UVRR system and detected the structural dynamics in the photoreactions of various proteins: the ligand photodissociation of carbonmonoxy myoglobin,[26,27] the primary protein response of photoactive yellow protein[28,29] and retinal proteins,[30,31] and the photoinduced electron transfer of glucose oxidase.[32] Accordingly, anti-Stokes UVRR spectra of aromatic amino acids with a time resolution of picoseconds should provide us information on the time evolution of the vibrational energy deposited in these residues in proteins.

In the present article, we discuss the results obtained by applying picosecond time-resolved anti-Stokes UVRR spectroscopy to the investigation of the vibrational energy flow in proteins. Specifically, we conducted test experiments to investigate the vibrational energy flow in ferric cytochrome *c*. Cytochrome *c* is a hemeprotein loosely associated with the inner membrane of the mitochondrion and an essential component of the electron transport chain there. It contains a heme group covalently bound to its polypeptide chain through cysteine residues. We chose cytochrome *c* because it has a single tryptophan residue (Trp59 in bovine cytochrome *c*) near the heme group. The ferric form of cytochrome *c* is considered to be photoinert, and hence, effective deposition of excess energy is possible through the photoexcitation of the heme unit. The time-resolved anti-Stokes UVRR spectra of Trp59 disclosed the kinetics of the energy flow from the heme group and the energy release of the residue in cytochrome *c*. Below, we discuss the kinetics of Trp59 in comparison with those for energy relaxation of the heme group and energy dissipation to water. We also discuss the advantages of the present technique for studying energy flow in proteins.

EXPERIMENTAL METHODS

Sample Preparation. Bovine heart cytochrome *c* was purchased from Sigma Aldrich (C2037). It was dissolved into a 40 mM phosphate buffer at pH 7.0 to prepare a 120 μM ferric cytochrome *c* solution. The buffer contained sodium sulfate (internal standard for Raman intensity), *n*-dodecyl β-D-maltoside, and bovine heart cytochrome *c* oxidase (CcO). The purified CcO was generously provided by Professor Takashi Ogura (University of Hyogo). We added 120 nM CcO to avoid the accumulation of a photoreduced product.

UVRR Measurements. Details of our UVRR apparatus have been described elsewhere.[27,28] The light source of our apparatus was a picosecond Ti:sapphire oscillator (Tsunami pumped by Millennia-Vs, Spectra-Physics) and amplifier (Spitfire pumped by Evolution-15, Spectra-Physics) system operating at 1 kHz. We pumped the heme in cytochrome *c* into either the S_1 or S_2 electronic excited state.

For the experiments using the 405 nm pump (S_2 excitation), the wavelength of the laser output was 810 nm. To generate the pump and probe pulses, the second harmonic of the laser output (405 nm) was divided into two parts. One portion of the 405 nm pulse was used as a pump pulse, which passed through an optical delay stage. The other portion was focused into a Raman shifter filled with methane gas to generate the first Stokes stimulated scattering at 460 nm. A probe pulse at 230 nm was generated as the second harmonic of the 460 nm output. The pump and probe pulses were collinearly overlapped and focused onto a flowing thin-film of the sample solution by a planoconvex lens. At the sample point, the energies of the pump and probe were 1.0 and 20 μJ, respectively. The cross-correlation width between the two pulses was 3.6 ps.

For the experiments with the 537 nm pump (S_1 excitation), the wavelength of the laser output was 778 nm. To generate the pump and probe pulses, the second harmonic of the laser output (389 nm) was divided into two parts. One portion of the 389 nm pulse passed through the optical delay stage and the optical parametric generation (OPG) and optical parametric amplification (OPA) devices.[33] A pump pulse at 537 nm was generated as the output of the OPG/OPA system. The other portion was focused into a Raman shifter filled with hydrogen gas to generate the first Stokes stimulated scattering at 464 nm. A probe pulse at 232 nm was generated as the second harmonic of the 464 nm output. At the sample point, the energies of the pump and probe were 1.2 and 20 μJ, respectively. The cross-correlation width between the two pulses was 3.2 ps.

The UVRR measurements were obtained at room temperature, and the sample solution was replaced with a fresh one every 200−240 min. Sample integrity after exposure to laser irradiation was confirmed using UV−vis absorption analysis. The Raman scattering light was collected and focused onto the entrance slit of a prefilter[34] coupled to a single spectrograph (500M, Spex) by two achromatic doublet lenses. The dispersed light was detected with a liquid nitrogen-cooled charge-coupled device (CCD) camera (SPEC-10:400B/LN, Roper Scientific). Raman shifts were calibrated with anti-Stokes Raman bands of cyclohexane and an aqueous solution of Trp. The spectral dispersion of the CCD camera was 3.0−3.5 cm^{-1}/pixel.

RESULTS

Time-Resolved Anti-Stokes UVRR Spectra with Excitation into the S_2 State. Figure 1 shows the time-resolved anti-Stokes UVRR difference spectra measured with pump and probe pulses of which the wavelengths were 405 and 230 nm, respectively. The top trace is a probe-only spectrum, which represents the anti-Stokes UVRR spectrum for ferric cytochrome *c*. Raman bands of the Trp and Tyr residues in the UVRR spectra were identified by comparison with UVRR spectra of the aqueous amino acid solutions. The mode assignments made by Harada and co-workers were adopted.[24] The top trace contains the UVRR bands for Trp at 759 (W18 mode), 876 (W17 mode), and 1015 cm^{-1} (W16 mode) and a band for Tyr at 1181 cm^{-1} (Y9a). The band at 1599 cm^{-1} is not assigned to any modes of aromatic amino acid residues. The band at 983 cm^{-1} indicated by the asterisk is due to the sulfate ion added as an internal standard for determining Raman intensity.

Difference spectra ascribed to vibrationally excited populations were calculated for cytochrome *c* excited into the S_2 electronic excited state as shown in Figure 1. For all of the difference spectra, the Raman bands of sulfate were used as an internal standard. The 405 nm pump pulse excited the heme into the S_2

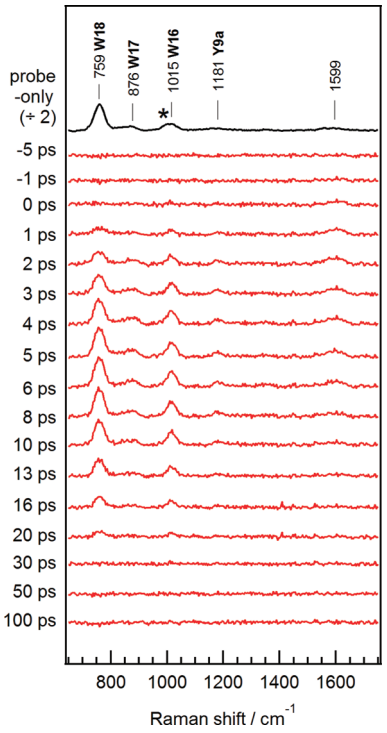

Figure 1. Time-resolved anti-Stokes UVRR spectra of ferric cytochrome *c* for time delays from −5 to 100 ps. Probe and pump wavelengths are 230 and 405 nm, respectively. The top trace is the probe-only spectrum corresponding to the anti-Stokes UVRR spectrum of ferric cytochrome *c* divided by a factor of 2. The other spectra are time-resolved difference spectra generated by subtracting the probe-only spectrum from the pump−probe spectrum at each delay time. The asterisk represents the sulfate band at 983 cm^{-1} as an intensity standard. The accumulation time for obtaining each spectrum is 116 min.

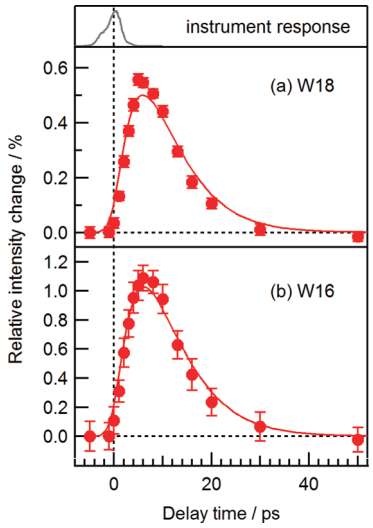

Figure 2. Temporal intensity changes of the anti-Stokes (a) W18 and (b) W16 bands in the range of −5 to 50 ps upon S_2 (405 nm) excitation. Circles indicate the band intensity measured at each delay time relative to the band intensity in the probe-only spectrum. Solid lines are the best-fits to a double exponential function of the form $I_1[\exp(-t/\tau_{decay}) - \exp(-t/\tau_{rise})]$ convoluted with the instrument respose function.

state. At a −5 ps delay, no difference features were observed for the Trp and Tyr Raman bands; this result corroborates the cross-correlation measurement of 3.6 ps. In contrast, the spectrum at 5 ps shows the pump-induced positive difference features observed for the Trp and Tyr anti-Stokes Raman bands, indicating pump-induced intensity changes. The Trp and Tyr bands disappeared within 30 ps in the anti-Stokes UVRR difference spectra. It should be noted that the sulfate band was completely eliminated in the time-resolved difference spectra. The temporal behavior of the integrated intensity of the W16 and W18 bands in the time-resolved difference spectra relative to those in the probe-only spectrum are shown in Figure 2. The intensity changes of the W16 and W18 bands were fitted by a convolution of the instrument response with an exponential rise and an exponential decay, $I_1[\exp(-t/\tau_{decay}) - \exp(-t/\tau_{rise})]$. The time constants of rise and decay for the W16 band were $5.6_7 \pm 3.0$ and $5.6_8 \pm 3.0$ ps, respectively. For the W18 band, the time constants of 5.5 ± 2.5 and 5.6 ± 2.5 ps were obtained for the rise and decay, respectively.

Time-Resolved Stokes UVRR Spectra. We observed the intensity rise and decay of the anti-Stokes UVRR bands of Trp upon the photoexcitation of the heme. The intensity changes of the anti-Stokes bands can result from changes in the population of the vibrational excited states and/or changes in the resonance Raman cross-sections of the modes. The resonance Raman cross-section can be affected by conformational changes of the side chain and/or environmental changes around the residue. If the anti-Stokes intensity changes result from a change in the cross-sections, the Stokes UVRR intensity must exhibit temporal changes with the same time constants as the anti-Stokes UVRR intensity. To verify this possibility, we measured the time-resolved Stokes UVRR spectra of ferric cytochrome *c* upon photoexcitation of the heme. As can be seen in Figure 3, upon photoexcitation of the heme, negative bands were observed in the time-resolved difference spectra. Figure 4a,b shows the temporal behaviors of the integrated intensity of the W16 and W18 bands, respectively. The intensity changes of these bands were fitted by $I_2 + I_3 \exp(-t/\tau_{Stokes})$. The curve fitting of the data demonstrated that the intensities of the W16 and W18 bands decreased within the instrument response time and recovered with time constants of 9.7 ± 0.8 and 9.8 ± 1.6 ps, respectively.

Figure 4c,d compares the changes of the integrated Stokes and anti-Stokes band intensities of the W16 and W18 bands, respectively. The temporal behaviors of the Stokes and anti-Stokes band intensities do not coincide with each other for either of the W16 and W18 bands. The Stokes intensity changed instantaneously upon photoexcitation, while the anti-Stokes intensity exhibited a delayed response. Accordingly, we concluded that the increase and decrease of the anti-Stokes band intensities represents the flow of excess energy from the heme to the Trp residue and the release from the Trp residue to the surroundings, respectively.

Time-Resolved Anti-Stokes UVRR Spectra with Excitation into the S_1 State. It is interesting to see how the kinetics of the flow of excess energy in the protein moiety depend on the amount of energy introduced. The heme shows two prominent absorption bands, the B band around 400 nm and the Q band in the 500−600 nm region. The transition of the B and Q bands corresponds to the S_2 and S_1 excitations, respectively. Measurements of time-resolved anti-Stokes UVRR spectra after the S_1 state excitation of the heme were performed to evaluate whether the amount of excess energy affects the kinetics of the energy flow in the protein moiety. Figure 5 shows the time-resolved anti-Stokes UVRR difference spectra measured with pump and probe

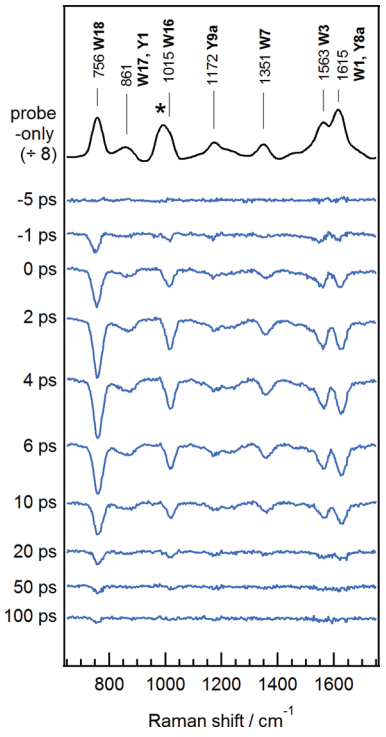

Figure 3. Time-resolved Stokes UVRR spectra of ferric cytochrome *c* for time delays from −5 to 100 ps. Probe and pump wavelengths are 230 and 405 nm, respectively. The top trace is the probe-only spectrum corresponding to the Stokes UVRR spectrum of ferric cytochrome *c* divided by a factor of 8. The other spectra are time-resolved difference spectra generated by subtracting the probe-only spectrum from the pump−probe spectrum at each delay time. The asterisk represents the sulfate band at 983 cm^{-1} as an intensity standard. The accumulation time for obtaining each spectrum is 20 min.

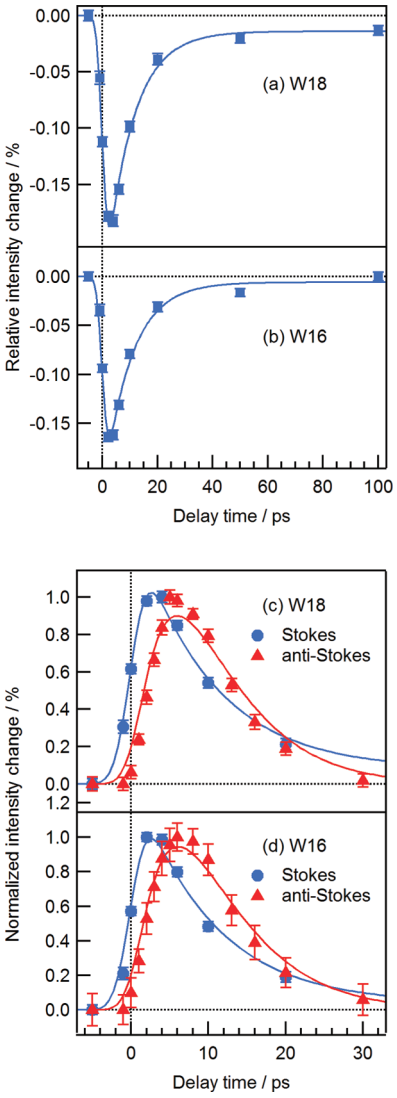

Figure 4. Temporal intensity changes of the Stokes (a) W18 and (b) W16 bands in the range of −5 to 100 ps upon S_2 (405 nm) excitation. Circles indicate the band intensity measured at each delay time relative to the band intensity in the probe-only spectrum. The solid lines are the best-fits to an exponential function of the form $I_2 + I_3 \exp(-t/\tau_{Stokes})$ convoluted with the instrument respose function. Panels c and d show the comparison of the temporal intensity changes of the Stokes (circles) and anti-Stokes (triangles) bands upon S_2 (405 nm) excitation. Intensity changes of W18 and W16 bands are shown in panels c and d, respectively. The solid lines are the best-fits to a function of the form $I_2 + I_3 \exp(-t/\tau_{Stokes})$ and $I_1[\exp(-t/\tau_{decay}) - \exp(-t/\tau_{rise})]$ for Stokes and anti-Stokes bands, respectively, convoluted with the instrument respose function.

pulses of which the wavelengths were 537 and 232 nm, respectively. As observed in the time-resolved anti-Stokes spectra of the S_2 state excitation, after photoexcitation of the heme, several Trp bands appeared in a few picoseconds and disappeared within tens of picoseconds in the anti-Stokes UVRR spectra. This behavior indicates that upon excitation into the S_1 excited state, the excess energy from the heme is transferred to the Trp residue and then released to the surroundings of the residue.

Figure 6 shows the temporal changes of the anti-Stokes W16 and W18 band intensities upon S_1 excitation. The solid lines are fitted using the same time constants obtained based on the data generated from the S_2 excitation. We were able to fit the observed data well for both the S_1 and S_2 excitations of the heme using the common time constant values. This result indicates that the kinetics of the flow of excess energy in the protein moiety are independent of the amount of energy.

DISCUSSION

Changes in the Stokes UVRR Difference Spectra. Upon S_2 photoexcitation of the heme, the Stokes UVRR bands of the Trp residue exhibited intensity bleaching and recovery. This variation indicates that the structure and/or environment of the Trp changed upon photoexcitation. There are possible reasons to account for the changes in the Stokes intensities: (1) changes in hydrogen bonding between the heme and the Trp residue, (2) ligand dissociation, (3) electron transfer from the Trp residue to the heme, and (4) population bleaching of the ground electronic state of the Trp residue by two-photon excitation.

Trp59 in cytochrome *c* forms a hydrogen bond with one of the propionic groups of the heme and is located in a hydrophobic environment as shown in Figure 7. The intensities of the UVRR W16 and W18 bands of the Trp residues are sensitive to changes in the hydrogen bonding of the residues and/or environmental changes in the residues.[35] It is often observed that vibrational excitation results in the dissociation of hydrogen bonds in associated liquids.[36−38] Thus, the vibrational excitation of the heme

dx.doi.org/10.1021/jp207500b |*J. Phys. Chem. B* 2011, 115, 13057–13064

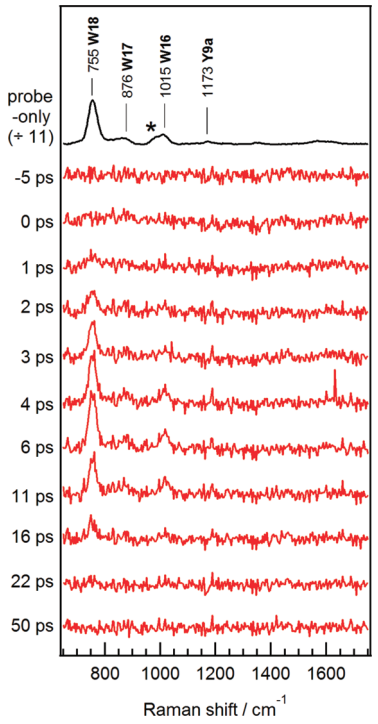

Figure 5. Time-resolved anti-Stokes UVRR spectra of ferric cytochrome *c* for time delays from −5 to 50 ps. Probe and pump wavelengths are 232 and 537 nm, respectively. The top trace is the probe-only spectrum corresponding to the anti-Stokes UVRR spectrum of ferric cytochrome *c* divided by a factor of 11. The other spectra are time-resolved difference spectra generated by subtracting the probe-only spectrum from the pump−probe spectrum at each delay time. The asterisk represents the sulfate band at 983 cm^{-1} as an intensity standard. The accumulation time for obtaining each spectrum is 190 min.

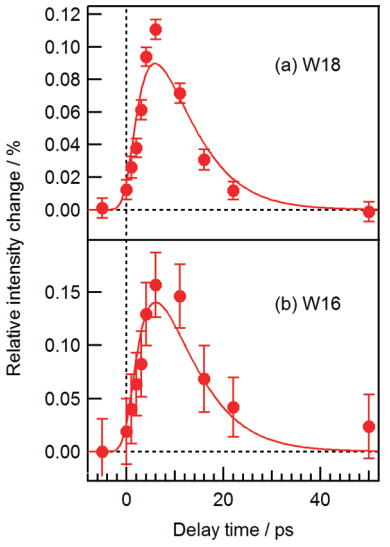

Figure 6. Temporal intensity changes of the anti-Stokes (a) W18 and (b) W16 bands in the range of −5 to 50 ps upon S_1 (537 nm) excitation. Circles indicate the band intensity measured at each delay time relative to the band intensity in the probe-only spectrum. Solid lines are the simulated curves using the function of $I_1'[\exp(-t/\tau_{decay}) - \exp(-t/\tau_{rise})]$ convoluted with the instrument response function. The values of τ_{rise} and τ_{decay} are fixed to those for time constants obtained based on the data generated from the S_2 excitation.

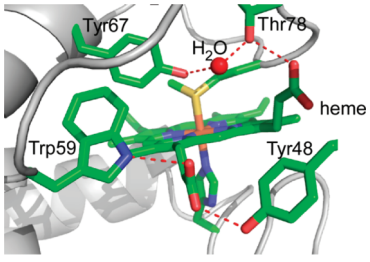

Figure 7. Crystallographic structure around the heme in ferric cytochrome *c* (PDB ID code 2B4Z). Dashed lines represent hydrogen bonds.

may cause the dissociation of the hydrogen bond between the heme propionate and Trp 59. This disruption would induce intensity changes of the UVRR W16 and W18 bands. Changes in the hydrogen bonding between the heme and Trp59 could therefore account for the changes in the Stokes UVRR intensities of Trp59.

It has been shown that ferrous cytochrome *c* exhibits photodissociation of the methionine ligated to the heme upon Soret photoexcitation (S_2 excitation) of the heme.[39] It is widely accepted, however, that ferric cytochrome *c* does not show photodissociation of the axial ligand. A time-resolved visible resonance Raman study indicated that the photodissociation of the ligand does not take place and that the relaxation dynamics are dominated by vibrational cooling in the ground electronic state.[40] More recently, a transient absorption study showed that the heme maintains its 6-fold coordination and that no global conformational relaxation was observed, again in contrast to ferrous cytochrome *c*.[41]

An electron transfer from the Trp residue to the heme could also result in the intensity changes of the Stokes UVRR bands. In fact, a recent time-resolved UVRR study of the photoinduced electron transfer of glucose oxidase showed intensity bleaching and recovery of the Trp bands, indicating the formation and decay of Trp cation radicals.[32] However, it is unlikely that the electron transfer is induced by the photoexcitation of the heme in ferric cytochrome *c*. First, the characteristic band of the Trp cation radical around 1520 cm^{-1} [42] was not observed in the time-resolved Stokes UVRR spectra of cytochrome *c*. Second, the photoinduced changes of hemeproteins have been extensively studied, and there has been no report of electron transfer from the Trp residue to the photoexcited heme group. Therefore, it is unlikely that the changes in the Stokes UVRR spectra are due to an electron transfer.

Although Trp residues do not have an absorption band at the 405 nm wavelength of the pump pulse, the residue can be excited by two-photon excitation. Two-photon excitation of the Trp residue by the 405 nm pump pulses could cause depletion of the population of the electronic ground state of the Trp residue. In fact, it has been shown that intense visible pulses cause a two-photon excitation of Trp.[43] To verify this possibility, we measured the dependence of the pump energy on the intensity change of the Stokes bands (see Figure S1 in the Supporting Information). The negative intensities in the Stokes UVRR difference spectra were proportional not to the square of the energy of the pump pulse but to the energy of the pump pulse. Thus, the two-photon excitation of the Trp residue cannot account for the intensity changes of the Stokes UVRR bands.

Accordingly, ligand dissociation, electron transfer from the Trp59 residue to the heme, and population bleaching of the

ground electronic state of the Trp59 residue by two-photon excitation do not explain the change of the Stokes Raman bands upon the photoexcitation. Changes in the hydrogen bonding between the heme and Trp59 is therefore the most likely explanation for the changes in the Stokes UVRR intensities of Trp59.

Kinetics of the Energy Flow. Temporal changes in the anti-Stokes intensity can be influenced by changes in the vibrational population and the cross-section. In the present measurements, the temporal changes of the vibrationally excited population must influence the anti-Stokes intensity of Trp59 because the temporal behaviors of the anti-Stokes bands were different from those of the Stokes bands. The intensity changes of the Stokes bands were not negligible, however, and indicated that the Raman cross-section was temporally changed in 0−40 ps. Therefore, the temporal change of the anti-Stokes intensity contains not only the contribution of the change in vibrational population but also the change in the cross-section. The contribution of the cross-section can be eliminated by appropriate correction methods.[44,45] In order to perform the correction, the contribution of the photoexcited molecules to the observed spectra must be extracted. In the present measurements, however, it is difficult to discriminate between the contributions of the photoexcited and unphotoexcited molecules to the Stokes intensity because there is no large difference between the Stokes spectra of the photoexcited and unphotoexcited molecules. Thus, we cannot exactly determine how large the fraction of the photoexcited molecules in the observation volume is and thus cannot exactly eliminate the contribution of the change in the cross-section. Instead, we estimated for the fraction of photoexcited molecules the time constants for the change of the vibrational population in several instances. I^0, $I^*(t)$, and f denote the band intensity of all unphotoexcited molecules in the observation volume in the absence of the pump pulse, the band intensity of the photoexcited molecules in the observation volume, and the fraction of the photoexcited molecules in the observation volume, respectively. The anti-Stokes intensity of the photoexcited molecules relative to the Stokes intensity of the photoexcited molecules, $I_{as}^*(t)/I_s^*(t)$, reflects the contribution of the vibrational population, where the subscripts s and as are for the Stokes and anti-Stokes intensities, respectively. The band intensities observed in the time-resolved difference spectra are represented by $I^*(t) - f \cdot I^0$ because the internal standard for the Raman intensity was used to correct for the intensity reduction due to self-absorption. Thus, the relative intensity changes are given by

$$\frac{I^*(t) - f \cdot I^0}{I^0} = \frac{I^*(t)}{I^0} - f \tag{1}$$

In the data analysis, the observed relative intensity changes of the Stokes bands were well fitted to the form $I_{Stokes}(t) = I_2 + I_3 \exp(-t/\tau_{Stokes})$. Therefore, the relative intensity of the photoexicited molecules is expressed as

$$\frac{I_s^*(t)}{I_s^0} = I_2 + I_3 \exp\left(-\frac{t}{\tau_{Stokes}}\right) + f \tag{2}$$

Similarly, for the anti-Stokes bands, the relative intensity is expressed as

$$\frac{I_{as}^*(t)}{I_{as}^0} = I_1\left[\exp\left(-\frac{t}{\tau_{decay}}\right) - \exp\left(-\frac{t}{\tau_{rise}}\right)\right] + f \tag{3}$$

Scheme 1. Energy Flow in Hemeproteins

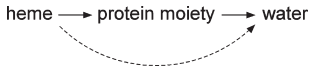

Combining eqs 2 and 3, we obtain the relationship

$$\frac{I_{as}^*(t)}{I_s^*(t)} \propto \frac{I_1\left[\exp\left(-\frac{t}{\tau_{rise}}\right) - \exp\left(-\frac{t}{\tau_{decay}}\right)\right] + f}{I_2 + I_3 \exp\left(-\frac{t}{\tau_{Stokes}}\right) + f} \tag{4}$$

We calculated the value of the right-hand side of eq 4 for $f = 0.3$, 0.4, 0.5, 0.6, and 0.7, and obtained time constants for the rise (τ_1) and decay (τ_2) components (see Figure S2 and Table S1 in the Supporting Information). These time constants characterize the changes in the vibrational populations of Trp59. It was found that the time constants of τ_1 and τ_2 are less sensitive to the value of f and are 1−3 and ∼8 ps, respectively.

The flow of the excess energy can schematically be described as shown in Scheme 1. The increase and decrease in the vibrational population of Trp59 corresponds to the inflow (τ_1) and outflow (τ_2) in Trp59 of the excess energy. In the present study, we determined the time constants to be 1−3 and ∼8 ps for the energy flow from the heme to the Trp and the energy release from the Trp, respectively. Time-resolved anti-Stokes visible resonance Raman spectroscopy revealed that the heme cooling in myoglobin takes place with a time constant of ∼2 ps.[18,19] We thus measured the time-resolved anti-Stokes visible resonance Raman spectra of ferric cytochrome *c* (see Figure S3 in the Supporting Information). The time constant of the heme cooling of ferric cytochrome *c* was estimated to be ∼2 ps based on the temporal change of the anti-Stokes band intensity (Figure S4 in the Supporting Information). This agrees with the time constant obtained with a molecular dynamics simulation.[46] The time constant of energy flow from the heme to Trp59 is comparable to that of heme cooling. This result is consistent if we assume that the energy is directly transferred to Trp59, although we cannot rule out a possibility that the energy is indirectly transferred to Trp59 via ultrafast channel. Next, we compared the time constant of the energy release from the Trp with that of the heating of water. In the time-resolved IR study for deoxy myoglobin, excess energy dissipation from the globin to the water bath was observed as a temperature increase of the water.[21] The temporal behavior of the water heating was explained using two components with time constants of 7.5 and ∼20 ps. The fast component was attributed to energy release to solvent water through heme propionates and/or through collective motions of the protein. The former possibility was supported by computational[46−48] and experimental studies[49−51] for myoglobin. In cytochrome *c*, the direct channel from the heme to solvent water is less efficient than that in myoglobin because the heme in cytochrome *c* has no propionate.[46] The slow component was attributed to the energy transfer from the heme to the solvent water through the protein via a classical diffusion process. Because the size and shape of cytochrome *c* are similar to those of myoglobin, it is likely that the time constant of water heating for cytochrome *c* is comparable to that of the slow component of myoglobin (∼20 ps). The time constant of the energy release from Trp59 is smaller than that of the slow component of water heating. This result is consistent with the supposition that the energy released from Trp59 is

transferred to solvent water through the remaining protein moiety and is also consistent with the energy flow as described in Scheme 1. The direct energy transfer from Trp59 to solvent water is very unlikely because Trp59 is buried inside the protein and is not exposed to solvent water.

Vibrational Cooling of the Tryptophan Residue. We observed the kinetics of vibrational heating and cooling of Trp59. The vibrational energy dynamics of molecules comparable with tryptophan have been studied by time-resolved spectroscopy. For example, it was shown that azulene exhibited vibrational cooling with time constants of 9.0 and 3.3 ps in ethanol and 25% aqueous methanol solution, respectively.[52] In *n*-alkanes, the cooling times decreased with increasing chain length from 12.5 ps in pentane to 10.8 ps in hexadecane. These data suggest that hydrogen bond formation has a strong influence on the thermalization process. The time constant of cooling of Trp59 is comparable with azulene in the hydrogen-bonded systems, suggesting that the mechanism of vibrational cooling in proteins is similar to that in associated liquids.

Advantage of the Present Technique for Studies on Intermolecular Vibrational Energy Transfer. Understanding the vibrational dynamics of polyatomic molecules in polyatomic solutions is central to many problems in chemistry, physics, and biology. Despite extensive experimental and theoretical investigations, one problem has, however, received very little attention due to experimental difficulties, namely, the intermolecular vibrational energy transfer between two different polyatomic molecules in solution. Vibrational energy transfer between a solute molecule and solvent molecules has been studied by various pump−probe techniques.[53−56] For instance, Iwaki and Dlott studied the vibrational energy relaxation of a methanol−CCl_4 mixture using mid-IR pump and anti-Stokes Raman probe experiments.[55] They excited the C−H and O−H stretching modes of methanol and probed the low-wavenumber CCl_4 Raman transitions. The buildup of CCl_4 excitation completed within about 20 ps. In these studies, however, the averages of energy transfer processes to many solvent molecules were observed. Selective observation is impossible for energy transfer between a specific pair of solute and solvent molecules for which distance and orientation are well-defined.

An attempt was made to observe the energy transfer between a pair of molecules by utilizing molecular heater−thermometer integrated systems, where two different molecules, namely, a heater that absorbs the visible radiation and a thermometer that probes the temperature by changing the absorption in the vicinity of its hot band, are brought into proximity by covalently linking the two discrete molecules.[57−59] However, for systems with longer linkers, the flexibility of the linker makes it difficult to keep the distance and relative orientation between the heater and thermometer molecules well-defined.

In hemeprotein, the distance and relative orientation between heme and the amino acid residues are well characterized based on X-ray crystallographic data, and the distance between heme and the amino acid residues can be as long as 20 Å. It is possible to observe how the energy deposited to the heme migrates to surrounding residues by measuring the anti-Stokes band intensities of the residues. Excess energy as great as 25000 cm^{-1} can be deposited into the heme by photoexcitation via the Soret transition. Accordingly, studies using the present technique based on hemeproteins will provide us new insights for understanding the mechanism of vibrational energy transfer in condensed phases.

CONCLUSION

Vibrational energy flow in ferric cytochrome *c* has been examined using picosecond time-resolved anti-Stokes UVRR experiments. By monitoring the anti-Stokes UVRR intensities of the Trp59 residue, the vibrationally excited population has been measured directly. It has been found from temporal changes of the anti-Stokes UVRR intensities that energy flow from the heme to Trp59 and energy release from Trp59 took place with time constants of 1−3 and ∼8 ps, respectively. The time constants of energy inflow and outflow are consistent with the constants associated with heme cooling and water heating as reported previously. Comparison of the data generated upon excitation to the two different electronic excited states showed that the kinetics of the energy flow were not affected by the amount of excess energy deposited to the heme group. These results demonstrate that the present technique is powerful for studying the vibrational energy exchange in proteins.

ASSOCIATED CONTENT

Supporting Information. Pump power dependence of the anti-Stokes UVRR bands, values of the right-hand side of eq 4, time constants for the rise and decay components on the right-hand side of eq 4, time-resolved anti-Stokes visible resonance Raman spectra, and the temporal changes of the anti-Stokes band intensities. This material is available free of charge via the Internet at http://pubs.acs.org.

AUTHOR INFORMATION

Corresponding Author

*Phone: +81-6-6850-5776. Fax: +81-6-6850-5776. E-mail: mztn@chem.sci.osaka-u.ac.jp.

ACKNOWLEDGMENT

This work was supported by a Grant-in-Aid for Scientific Research in the Priority Area Molecular Science for Supra Functional Systems (Grant No. 19056013) to Y.M. from the Ministry of Education, Science, Sports and Culture of Japan and a Grant-in-Aid for Scientific Research (B) (Grant No. 20350007) to Y.M. from the Japan Society for the Promotion of Science. We thank Professor Takashi Ogura (University of Hyogo) for his generous gift of the purified CcO sample.

REFERENCES

(1) Elsaesser, T.; Kaiser, W. *Annu. Rev. Phys. Chem.* **1991**, *42*, 83–107.
(2) Laubereau, A.; Kaiser, W. *Rev. Mod. Phys.* **1978**, *50*, 607–665.
(3) Owrutsky, J. C.; Raftery, D.; Hochstrasser, R. M. *Annu. Rev. Phys. Chem.* **1994**, *45*, 519–555.
(4) Oxtoby, D. W. *Annu. Rev. Phys. Chem.* **1981**, *32*, 77–101.
(5) Seilmeier, A.; Kaiser, W. *Ultrashort Laser Pulses*; Kaiser, W., Ed.; Springer: New York, 1993; pp 279−317.
(6) Zinth, W.; Kaiser, W. *Ultrashort Laser Pulses*; Kaiser, W., Ed.; Springer: New York, 1993; pp 235−277.
(7) Frauenfelder, H.; Wolynes, P. *Science* **1985**, *229*, 337–345.
(8) Henry, E. R.; Eaton, W. A.; Hochstrasser, R. M. *Proc. Natl. Acad. Sci. U.S.A.* **1986**, *83*, 8982–8986.
(9) Elber, R.; Karplus, M. *Science* **1987**, *235*, 318–321.
(10) Miller, R. J. D. *Annu. Rev. Phys. Chem.* **1991**, *42*, 581–614.
(11) Miller, R. J. D. *Acc. Chem. Res.* **1994**, *27*, 145–150.
(12) Onuchic, J. N.; Wolynes, P. G. *J. Chem. Phys.* **1993**, *98*, 2218–2224.

(13) Sumi, H. *J. Phys. Chem.* **1991**, *95*, 3334–3350.
(14) Champion, P. M.; Lange, R. *J. Chem. Phys.* **1980**, *73*, 5947–5957.
(15) Dlott, D. D. *J. Opt. Soc. Am. B* **1990**, *7*, 1638–1652.
(16) Lingle, R.; Xu, X.; Zhu, H.; Yu, S. C.; Hopkins, J. B.; Straub, K. D. *J. Am. Chem. Soc.* **1991**, *113*, 3992–3994.
(17) Petrich, J. W.; Martin, J. L.; Houde, D.; Poyart, C.; Orszag, A. *Biochemistry* **1987**, *26*, 7914–7923.
(18) Mizutani, Y.; Kitagawa, T. *Science* **1997**, *278*, 443–446.
(19) Mizutani, Y.; Kitagawa, T. *Chem. Rec.* **2001**, *1*, 258–275.
(20) Li, P.; Sage, J. T.; Champion, P. M. *J. Chem. Phys.* **1992**, *97*, 3214–3227.
(21) Lian, T.; Locke, B.; Kholodenko, Y.; Hochstrasser, R. M. *J. Phys. Chem.* **1994**, *98*, 11648–11656.
(22) Genberg, L.; Bao, Q.; Gracewski, S.; Miller, R. J. D. *Chem. Phys.* **1989**, *131*, 81–97.
(23) Genberg, L.; Heisel, F.; McLendon, G.; Miller, R. J. D. *J. Phys. Chem.* **1987**, *91*, 5521–5524.
(24) Harada, I.; Takeuchi, H. Raman and Ultraviolet Resonance Raman Spectra of Proteins and Related Compounds. In *Spectroscopy of Biological Systems*; Clark, R. J. H., Hester, R. E., Eds.; John Wiley & Sons: Chichester, U.K., 1986; pp 113−175.
(25) Kitagawa, T.; Hirota, S. Raman Spectroscopy of Proteins. In *Handbook of Vibrational Spectroscopy*; Chalmers, J. M., Griffiths, P. R., Eds.; John Wiley & Sons: Chichester, U.K., 2002; Vol. 5, pp 3426−3446.
(26) Sato, A.; Gao, Y.; Kitagawa, T.; Mizutani, Y. *Proc. Natl. Acad. Sci. U.S.A.* **2007**, *104*, 9627–9632.
(27) Sato, A.; Mizutani, Y. *Biochemistry* **2005**, *44*, 14709–14714.
(28) Mizuno, M.; Hamada, N.; Tokunaga, F.; Mizutani, Y. *J. Phys. Chem. B* **2007**, *111*, 6293–6296.
(29) Mizuno, M.; Kamikubo, H.; Kataoka, M.; Mizutani, Y. *J. Phys. Chem. B* **2011**, *115*, 9306–9310.
(30) Mizuno, M.; Shibata, M.; Yamada, J.; Kandori, H.; Mizutani, Y. *J. Phys. Chem. B* **2009**, *113*, 12121–12128.
(31) Mizuno, M.; Sudo, Y.; Homma, M.; Mizutani, Y. *Biochemistry* **2011**, *50*, 3170–3180.
(32) Fujiwara, A.; Mizutani, Y. *J. Raman Spectrosc.* **2008**, *39*, 1600–1605.
(33) Uesugi, Y.; Mizutani, Y.; Kitagawa, T. *Rev. Sci. Instrum.* **1997**, *68*, 4001–4008.
(34) Kaminaka, S.; Mathies, R. A. *Appl. Spectrosc.* **1998**, *52*, 469–473.
(35) Chi, Z.; Asher, S. A. *J. Phys. Chem. B* **1998**, *102*, 9595–9602.
(36) Graener, H.; Ye, T. Q.; Laubereau, A. *J. Chem. Phys.* **1989**, *90*, 3413–3416.
(37) Graener, H.; Ye, T. Q.; Laubereau, A. *J. Chem. Phys.* **1989**, *91*, 1043–1046.
(38) Asbury, J. B.; Steinel, T.; Fayer, M. D. *J. Phys. Chem. B* **2004**, *108*, 6544–6554.
(39) Wang, W.; Ye, X.; Demidov, A. A.; Rosca, F.; Sjodin, T.; Cao, W.; Sheeran, M.; Champion, P. M. *J. Phys. Chem. B* **2000**, *104*, 10789–10801.
(40) Negrerie, M.; Cianetti, S.; Vos, M. H.; Martin, J.-L.; Kruglik, S. G. *J. Phys. Chem. B* **2006**, *110*, 12766–12781.
(41) Stevens, J. A.; Link, J. J.; Kao, Y.-T.; Zang, C.; Wang, L.; Zhong, D. *J. Phys. Chem. B* **2010**, *114*, 1498–1505.
(42) Johnson, C. R.; Ludwig, M.; Asher, S. A. *J. Am. Chem. Soc.* **1986**, *108*, 905–912.
(43) Anderson, B. E.; Jones, R. D.; Rehms, A. A.; Ilich, P.; Callis, P. R. *Chem. Phys. Lett.* **1986**, *125*, 106–112.
(44) Okamoto, H.; Nakabayashi, T.; Tasumi, M. *J. Phys. Chem. A* **1997**, *101*, 3488–3493.
(45) Schomacker, K. T.; Bangcharoenpaurpong, O.; Champion, P. M. *J. Chem. Phys.* **1984**, *80*, 4701–4717.
(46) Bu, L.; Straub, J. E. *J. Phys. Chem. B* **2003**, *107*, 10634–10639.
(47) Okazaki, I.; Hara, Y.; Nagaoka, M. *Chem. Phys. Lett.* **2001**, *337*, 151–157.
(48) Sagnella, D. E.; Straub, J. E. *J. Phys. Chem. B* **2001**, *105*, 7057–7063.
(49) Gao, Y.; Koyama, M.; El-Mashtoly, S. F.; Hayashi, T.; Harada, K.; Mizutani, Y.; Kitagawa, T. *Chem. Phys. Lett.* **2006**, *429*, 239–243.
(50) Koyama, M.; Neya, S.; Mizutani, Y. *Chem. Phys. Lett.* **2006**, *430*, 404–408.
(51) Ye, X.; Demidov, A.; Rosca, F.; Wang, W.; Kumar, A.; Ionascu, D.; Zhu, L.; Barrick, D.; Wharton, D.; Champion, P. M. *J. Phys. Chem. A* **2003**, *107*, 8156–8165.
(52) Schwarzer, D.; Troe, J.; Votsmeier, M.; Zerezke, M. *J. Chem. Phys.* **1996**, *105*, 3121–3131.
(53) Deàk, J. C.; Pang, Y.; Sechler, T. D.; Wang, Z.; Dlott, D. D. *Science* **2004**, *306*, 473–476.
(54) Hong, X.; Chen, S.; Dlott, D. D. *J. Phys. Chem.* **1995**, *99*, 9102–9109.
(55) Iwaki, L. K.; Dlott, D. D. *J. Phys. Chem. A* **2000**, *104*, 9101–9112.
(56) Seifert, G.; Zurl, R.; Patzlaff, T.; Graener, H. *J. Chem. Phys.* **2000**, *112*, 6349–6354.
(57) Okazaki, T.; Hirota, N.; Nagata, T.; Osuka, A.; Terazima, M. *J. Am. Chem. Soc.* **1999**, *121*, 5079–5080.
(58) Okazaki, T.; Hirota, N.; Nagata, T.; Osuka, A.; Terazima, M. *J. Phys. Chem. A* **1999**, *103*, 9591–9600.
(59) Velate, S.; Danilov, E. O.; Rodgers, M. A. J. *J. Phys. Chem. A* **2005**, *109*, 8969–8975.

NOTE ADDED AFTER ASAP PUBLICATION

This paper was published ASAP on October 5, 2011. Equation 3 was updated. The correct version was published on October 17, 2011.